



## Particle and field characteristics of broadband electrons observed by the FAST satellite during a geomagnetic storm

A. Nakajima,<sup>1</sup> K. Shiokawa,<sup>1</sup> K. Seki,<sup>1</sup> R. J. Strangeway,<sup>2</sup> J. P. McFadden,<sup>3</sup> and C. W. Carlson<sup>3</sup>

Received 21 November 2006; revised 2 February 2007; accepted 27 February 2007; published 14 June 2007.

[1] Broadband electrons (BBEs) are remarkable flux enhancements ( $>10^{13}$  eV cm<sup>-2</sup> s<sup>-1</sup>) of precipitating electrons over a broad energy range (0.03–30 keV) near the equatorward edge of the auroral oval during geomagnetic storms. We show characteristics of particles (energy spectra and pitch angle distribution) and fields (electric field, magnetic field, and wave spectra) during a BBE event observed by the Fast Auroral Snapshot (FAST) satellite. The BBEs were observed at an altitude of  $\sim 2000$  km at  $59^{\circ}$ – $61^{\circ}$  invariant latitudes (ILATs) and 21 h magnetic local time (MLT). The event was observed at  $\sim 7$  min after the onset of a substorm during the main phase of the Bastille Day geomagnetic storm (minimum  $Dst = -301$  nT) on 15 July 2000. The precipitation region of the BBEs corresponded to a localized intensification of auroral emission, lasting  $\sim 14$  min, observed by the Polar UVI images at  $50^{\circ}$ – $60^{\circ}$  geomagnetic latitudes (MLATs) and 20–21 MLTs. These results suggest that rapid particle acceleration was occurring in the inner magnetosphere associated with a storm-time substorm. The pitch angle distribution of BBEs was isotropic except for a loss cone feature around the field-aligned upward direction at a higher energy range above  $\sim 1$  keV, while field-aligned electron fluxes were larger than the perpendicular fluxes below  $\sim 1$  keV. These results imply that a higher energy part of the BBEs originated from higher altitudes in the inner magnetosphere and that a lower energy part was accelerated parallel to the local magnetic field at lower altitudes near the satellite. Intense fluctuations of electric and magnetic fields were observed during this BBE event. From these results, we discuss possible acceleration of the lower energy part of BBEs through wave–particle interaction.

**Citation:** Nakajima, A., K. Shiokawa, K. Seki, R. J. Strangeway, J. P. McFadden, and C. W. Carlson (2007), Particle and field characteristics of broadband electrons observed by the FAST satellite during a geomagnetic storm, *J. Geophys. Res.*, *112*, A06220, doi:10.1029/2006JA012184.

### 1. Introduction

[2] Precipitation of auroral particles becomes very active and expands into lower latitudes during geomagnetic storms [e.g., *Gussenhoven et al.*, 1981; *Spiro et al.*, 1982]. *Hardy et al.* [1985] studied the global pattern of auroral electron precipitation as a function of geomagnetic activity using the  $Kp$  index. They showed that the low-latitude boundary of the auroral precipitating region moves equatorward continuously, and electron energy flux into the auroral oval increases at night side with increasing  $Kp$ . It is very important to investigate the acceleration and energization of auroral

electrons during active geomagnetic conditions to understand the process of energy transport from the magnetosphere to the ionosphere. Energy spectra of auroral electrons provide much useful information for investigating the acceleration and energization of auroral electrons. Auroral electron spectra during geomagnetic storms have been studied by several researchers [e.g., *Egeland et al.*, 1994; *Sharber et al.*, 1998; *Chen et al.*, 2005]. *Denig and Rich* [1986] concluded that electron distribution during a geomagnetic storm did not evidence acceleration by field-aligned electric potential difference by using the electron distribution observed by the S3–2 satellite. These results are still insufficient for a complete understanding of the characteristics of auroral electron spectra during geomagnetic storms.

[3] *Shiokawa et al.* [1996] found a characteristic spectrum of auroral electrons, named broadband electrons (BBEs), from observations by the Defense Meteorological Satellite Program (DMSP) satellites during storm-time substorms. BBEs are drastically intense flux ( $>10^{13}$  eV cm<sup>-2</sup> s<sup>-1</sup>) of precipitating electrons over a broad energy range (0.03–30 keV) near the equatorward edge of the auroral oval.

<sup>1</sup>Solar-Terrestrial Environment Laboratory, Nagoya University, Toyokawa, Japan.

<sup>2</sup>Institute of Geophysics and Planetary Physics, University of California Los Angeles, Los Angeles, California, USA.

<sup>3</sup>Space Sciences Laboratory, University of California Berkeley, Berkeley, California, USA.

Their magnetospheric source lies within the inner part of the plasma sheet. They are observed at  $47^{\circ}$ – $66^{\circ}$  geomagnetic latitudes (MLATs) with latitudinal widths of  $2^{\circ}$ – $9^{\circ}$  [Shiokawa *et al.*, 1997]. Shiokawa *et al.* [1999] reported a BBE event during which the DMSP satellites and the Combined Release and Radiation Effects Satellite (CRRES) were located in the same local time. In the CRRES altitude at  $L \sim 6$ , electron flux was enhanced drastically at energies of 0.1–10 keV, particularly in the field-aligned direction, and low-frequency electrostatic waves below 300 Hz were intensified. In these previous studies, BBEs were investigated using energy spectra obtained by the DMSP satellites. However, the DMSP satellites did not measure the pitch angle distribution of precipitating electrons.

[4] In this paper, we investigate characteristics of BBEs observed by the Fast Auroral SnapshoT (FAST) satellite on 15 July 2000. The FAST satellite measures pitch angle distribution of electrons and ions. In addition, the electric and magnetic fields and plasma waves are simultaneously measured. Their relationship to the geomagnetic storm and substorm is also investigated using ground geomagnetic field data. Global auroral images obtained by the Polar satellite enable us to investigate the temporal and spatial extent of BBEs for this event.

## 2. Observation Overview

### 2.1. The Fast Satellite

[5] The FAST satellite was launched on 21 August 1996, into an  $83^{\circ}$  inclination elliptical and polar orbit of  $350 \times 4175$  km. The orbital period is  $\sim 133$  min. The satellite crosses the auroral zone four times per orbit over a wide range of altitudes and local times. The satellite is spin-stabilized with a spin period of 5 s and is oriented in a “cart-wheel” attitude, with the spin axis nearly normal to the orbital plane [Carlson *et al.*, 1998]. In this paper, we use FAST data obtained by the electrostatic analyzers (ESAs) [Carlson *et al.*, 2001], the electric field instrument [Ergun *et al.*, 2001], and the magnetic field instrument [Elphic *et al.*, 2001]. The energy range of ESAs is 0.004–32 keV for electrons and 0.003–24 keV for ions.

[6] Figure 1 shows energy–time spectrograms of downward electrons (pitch angles within  $\pm 15^{\circ}$ ) for three sequential passes of the FAST satellite in the northern hemisphere at 2010:30–2017:30 universal time (UT) (Figure 1a), 2219:30–2226:30 UT (Figure 1b), and 2429:30–2436:30 UT (Figure 1c) on 15 July 2000. BBEs were observed at 2219:30–2220:55 UT,  $59^{\circ}$ – $61^{\circ}$  invariant latitudes (ILATs), and 21 h magnetic local time (MLT) (Figure 1b). During the time interval of the BBEs, the precipitating electron fluxes significantly increased over a wide energy range (0.005–30 keV) in the equatorward part of the auroral precipitation region. The FAST satellite terminated particle observation at latitudes lower than those shown in Figure 1b. At latitudes higher than the BBEs at 2220:55–2225:10 UT, the energy spectra showed features of plasma sheet electrons. The energy fluxes at 2220:55–2223:20 UT at  $62^{\circ}$ – $66^{\circ}$  ILAT were more intense than those at 2223:20–2225:10 UT at  $66^{\circ}$ – $70^{\circ}$  ILAT. An energy spectrum similar to the BBE was observed at 2223:16 UT in a short time interval of less than 2.5 s, which is the time resolution of the electron data.

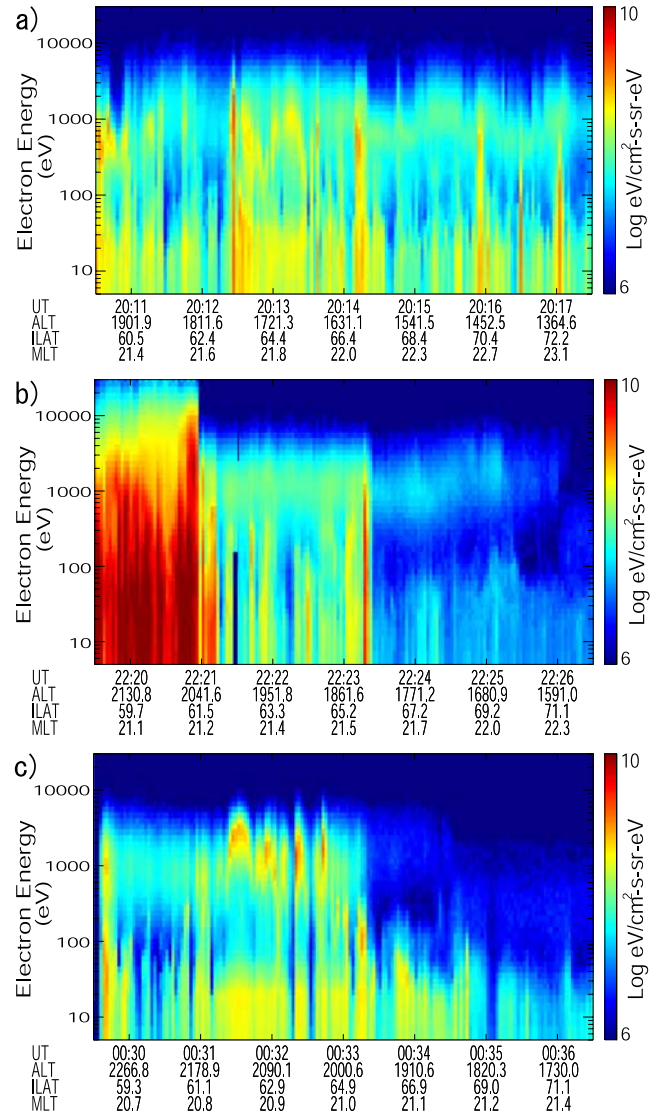


**Figure 1.** Energy–time spectrograms of downward electrons (pitch angles within  $\pm 15^{\circ}$ ) of three sequential passes of FAST in the northern hemisphere at (a) 2010:30–2017:30 universal time (UT), (b) 2219:30–2226:30 UT, and (c) 2429:30–2436:30 UT on 15 July 2000, including the BBEs at 2219:30–2220:55 UT in the middle panel (b). UT and satellite locations are shown at the bottom of each panel, where ALT, ILAT, and MLT denote altitude, invariant latitude, and magnetic local time, respectively. The FAST satellite traverses approximately the same ILAT and MLT every  $\sim 133$  min.

[7] The FAST satellite crossed nearly the same ILAT and MLT in the same hemisphere every  $\sim 133$  min. BBEs were not observed in one orbit before and after the BBE event, as shown in Figures 1a and 1c, respectively. Several inverted-V structures, which indicate the acceleration of electrons by a field-aligned electric potential difference [Frank and Ackerson, 1971], were observed in these passes. From these successive particle data, we conclude that the duration of the BBEs was less than  $\sim 4$  hours.

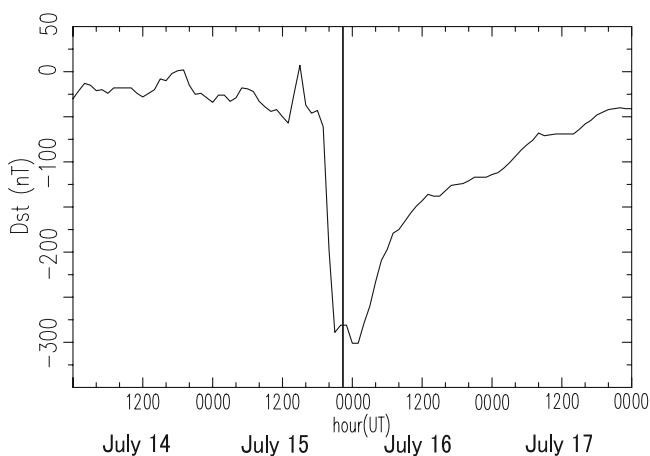


**Figure 2.** The  $Dst$  index on 14–17 July 2000. The vertical solid line indicates the time when the BBEs were observed by the FAST satellite.

## 2.2. Ground-Based Observations

[8] Figure 2 shows the variation of the  $Dst$  index on 14–17 July 2000. A geomagnetic storm started at 1500 UT on 15 July. The  $Dst$  index reached a minimum of  $-301$  nT at 0000 UT on 16 July. This storm is called the Bastille Event and has been extensively studied by several researchers [e.g., *Rastätter et al.*, 2002; *Nishino et al.*, 2006]. The vertical line indicates the time when the BBEs were observed, as shown in Figure 1b. The BBEs were observed during the main phase of this large geomagnetic storm at 2220 UT on 15 July, when the  $Dst$  index was  $-289$  nT.

[9] To investigate the relationship between the BBEs and the substorm, we show the H-component geomagnetic field variations observed at the ground-based stations at 2100–2400 UT on 15 July 2000, at around 21 MLT in the European sector (Figure 3). These stations were in the same local time where the BBEs were observed by the FAST satellite. From top to bottom, the data are plotted from high latitudes in the northern to low latitudes in the southern hemisphere. The vertical solid line in Figure 3 indicates the time when the BBEs were observed by the FAST satellite at 2220 UT.

[10] The H-component magnetic fields increased at low latitudes [Bangui (BNG), Tsumeb (TSU), and Hermanus (HER)] and decreased at high latitudes [Eskdalemuir (ESK) and Wingst (WNG)] from 2213 UT, as shown by the vertical dashed line, indicating that a substorm took place at this time. We also checked the Pi 2 magnetic pulsations to determine the timing of the substorm onset, using high time-resolution (1 s) magnetic field data obtained at HER. Four Pi 2 wave packets were identified at 2208, 2213, 2228, and 2236 UT. These results clearly show that a storm-time substorm started at 2213 UT, which is  $\sim 7$  min before the FAST observation of the BBEs. This fact is consistent with previous results about BBEs by *Shiokawa et al.* [1996, 1997, 1999]. The fact that the second Pi 2 corresponds to the global substorm onset with positive and negative H bays is consistent with the idea of consecutive Pi 2 bursts by *Cheng et al.* [2002, 2004].

[11] We used the high time-resolution magnetic field data only at HER because high time-resolution data are not

available at other stations in this local time sector. However, the Pi 2 pulsation is a global indicator of the expansion phase onset of substorm [*Yumoto et al.*, 1989]. Longitudinal and latitudinal time delays of the Pi 2 signature among ground stations are within 100 s [*Yumoto and the CPMN Group*, 2001].

## 2.3. Polar Satellite

[12] During the present event, the Polar satellite took auroral images by the Ultraviolet Imager (UVI) every 36–37 s [*Torr et al.*, 1995]. The UVI auroral images are used for comparison of BBEs with the region of auroral emission to investigate temporal and spatial variations of the BBEs.

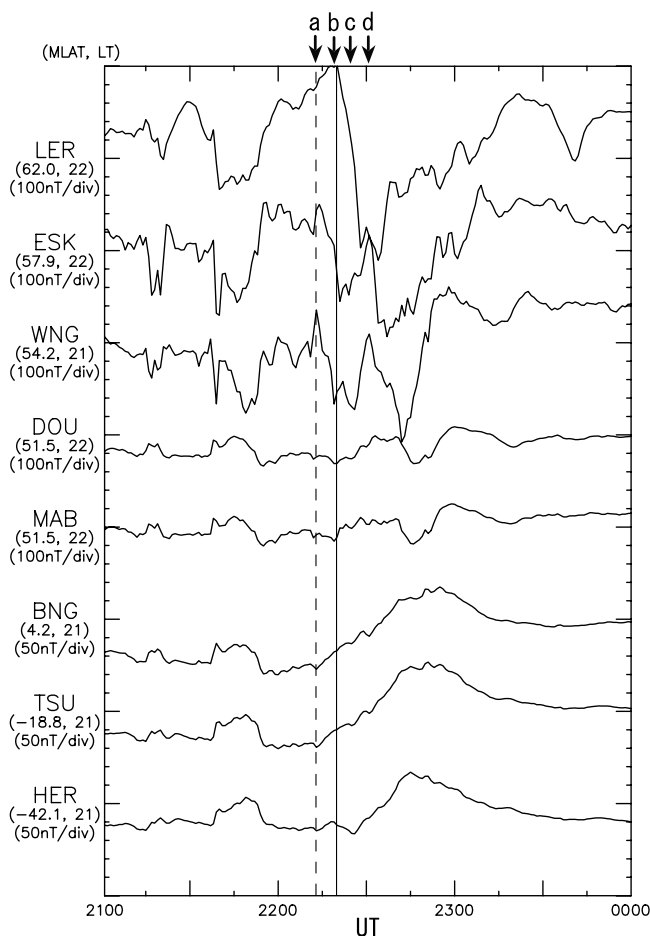


**Figure 3.** Geomagnetic H-component variations observed at the ground stations in the European sector at 2100–2400 UT on 15 July 2000. From top to bottom, the data are plotted from high latitudes in the northern hemisphere to low latitudes and to the southern hemisphere, Lerwick (LER), Eskdalemuir (ESK), Wingst (WNG), Dourbes (DOU), Manhay (MAB), Bangui (BNG), Tsumeb (TSU), and Hermanus (HER). These stations were in the same local time ( $\sim 21$  MLT) with the BBEs. The vertical solid line indicates the time when the BBEs were observed by the FAST satellite. The vertical dashed line indicates the onset time of a substorm (2213 UT). The arrows a–d indicate the times for which the Polar UVI images are shown in Figure 4.

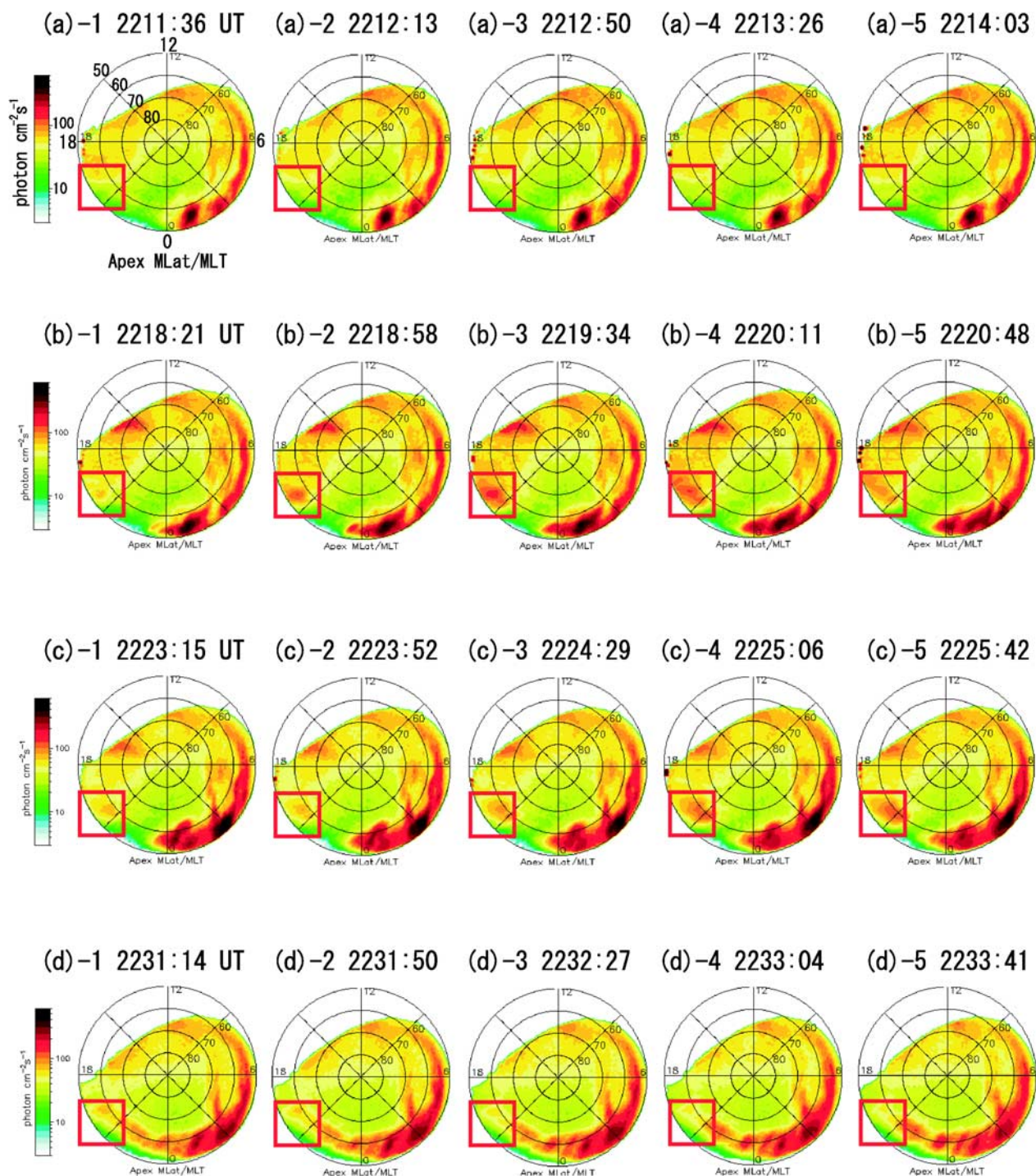


**Figure 4.** Sequential auroral UVI images observed by the Polar satellite every 36–37 s in the MLT–MLAT maps at (a) 2211:36–2214:03 UT, (b) 2218:21–2220:48 UT, (c) 2223:15–2225:42 UT, and (d) 2231:14–2233:41 UT on 15 July 2000. These times are indicated by arrows in Figure 3. The center and the largest circle indicate the north geomagnetic pole and 50° MLAT, respectively. The top and left sides of each panel are toward noon (12 MLT) and dusk side (18 MLT), respectively. The FAST satellite observed the BBEs at the region surrounded by the red squares.

[13] In Figure 4, Polar UVI images are displayed every 36–37 s in the MLT–MLAT maps at (a) 2211:36–2214:03 UT, (b) 2218:21–2220:48 UT, (c) 2223:15–2225:42 UT, and (d) 2231:14–2233:41 UT on 15 July 2000. These times are indicated by arrows in Figure 3. The

center and largest circles indicate the north geomagnetic pole and 50° MLAT, respectively. An intensification of auroral emission started at 2218:21 UT at 50°–60° MLAT and 20–21 MLT (Figure 4b). The BBEs were observed by the FAST satellite at 2219:30–2220:55 UT, at 59°–61° ILAT and

21 MLT, which was 1–2 min after this auroral intensification at 21 MLT in Figure 4b. The precipitating region of the BBEs corresponds to this local intensification of UVI auroral emission at  $50^{\circ}$ – $60^{\circ}$  MLAT and 20–21 MLT, surrounded by the red squares in Figure 4. Auroral intensification, corresponding to the substorm onset at 2213 UT (Figure 3), was not identified around the same region in Figure 4a. This may be because the corresponding auroral intensification at 2213 UT occurred at lower latitude which was not covered by the Polar data, since the local intensification in Figure 4b at 2218:21 UT was observed around the edge in a field of view of the Polar satellite. The auroral intensification in Figure 4b reached a peak at 2219:34 UT. The emission weakened and intensified again at 2223:52 UT in the same region in Figure 4c. This emission region was connected to the other emission region extended from the dawn sector and finally disappeared at 2232:27 UT (Figure 4d). The intensification lasted  $\sim 14$  min between 2218:21 UT and 2232:27 UT, suggesting the duration of  $\sim 14$  min of the BBEs.

### 3. Detailed Analyses of the Fast Data

#### 3.1. Summary of the Fast Data

[14] Figure 5 shows particle and field data obtained by the FAST satellite including the BBE event in Figure 1b at 2219:30–2224:00 UT on 15 July 2000. From top to bottom, the energy–time spectrograms and pitch angle distributions of electrons and ions, the electric and magnetic field fluctuations, and the wave spectra are shown. The FAST satellite was at altitudes of 2100–1800 km,  $59^{\circ}$ – $67^{\circ}$  ILAT, and 21–22 MLT. The time resolutions of the FAST data were 2.5 s (particle), 0.03 s (electric field), and 0.12 s (magnetic field) during this event. We do not discuss the data of electrons and ions at an energy range below 0.05 keV because these data are strongly affected by variations of satellite potential.

[15] The BBEs were observed at 2219:30–2220:55 UT,  $59^{\circ}$ – $61^{\circ}$  ILAT, and 21 MLT (Figure 5a). Figures 5b and 5c show the pitch angle distributions ( $0^{\circ}$  is field-aligned downward) of electrons at energy ranges above and below 1 keV, respectively. During the BBE event, Figure 5b shows that electron fluxes above 1 keV show isotropic features except around upward directions between  $130^{\circ}$  and  $230^{\circ}$ . At the upward directions, the fluxes significantly decrease, suggesting a loss cone feature. For electrons with energies below 1 keV in Figure 5c, downward parallel fluxes are most intense.

[16] Figures 5d and 5e show the energy–time spectrograms of ions for all the pitch angles and pitch angle distributions of ions, respectively. The ion fluxes above 10 keV were enhanced during the BBE event, while more intense fluxes were observed at energies below  $\sim 1$  keV. These ion components may be accelerated or heated associated with the BBEs. The intense ion fluxes below  $\sim 1$  keV correspond to the perpendicular fluxes in Figure 5e. Figure 5e also shows a single loss cone signature without upward ion fluxes during this event. Downward loss cone may be filled by pitch angle scattering of ions occurred in the taillike magnetic field region.

[17] Figure 5f shows variations of electric field intensity along the spacecraft velocity (nearly north–south, northward positive) perpendicular to the local magnetic field given by the International Geomagnetic Reference Field

(IGRF) model. Figure 5g shows the three components of the magnetic field variations in the field-aligned coordinate system. The blue line, which is labeled “b”, indicates the magnetic field variations along the model local magnetic field. The green line, which is labeled “ $p(\mathbf{B} \times \mathbf{V})$ ”, is the magnetic field along the direction defined by the cross-product  $\mathbf{B} \times \mathbf{V}$  (nearly east–west, eastward positive), where  $\mathbf{B}$  and  $\mathbf{V}$  are the local magnetic field and the spacecraft velocity vectors, respectively. The last component, labeled “ $v((\mathbf{B} \times \mathbf{V}) \times \mathbf{B})$ ”, is the magnetic field along the spacecraft velocity vector (nearly north–south). In Figures 5f and 5g, amplitudes of electric and magnetic field fluctuations are very large during the BBE event. The amplitudes of the electric and magnetic fields reach  $\sim 200$  mV/m and  $\sim 500$  nT, respectively. In Figure 5h, we show the wave power of the electric field at 0.016–16 kHz observed by the 56-m tip-to-tip antenna of the FAST satellite. The wave power was significantly intensified over the broad frequency range, particularly at around 2220:10 and 2220:45 UT during the BBE event.

[18] In the next five subsections, we show detailed analyses of these particle and field data.

#### 3.2. Field-Aligned Currents

[19] By using the magnetic field data in Figure 5g, we estimate the direction of field-aligned currents (FACs) during the BBE event at 2219:30–2220:55 UT and at higher latitudes at 2220:55–2223:20 UT, as shown by arrows and thick lines (red is upward and blue is downward). By assuming east–west sheet currents in the auroral oval, we are able to identify the direction (upward or downward) of FACs from the latitudinal gradient of magnetic field variations in the component of  $p(\mathbf{B} \times \mathbf{V})$  (green line, nearly east–west). The direction of the FACs shown in Figure 5g drastically changed during the BBE event. The FAST magnetic field data also show the complicated regions of both upward and downward currents at latitudes lower than the uniform downward current region. This result may indicate that the BBEs occurred equatorward of the steady downward current region in the premidnight sector. When we estimated FACs using particle data in the energy range of 0.08–30 keV (not shown), the direction was always upward during the BBE event. The discrepancy of FAC directions between those calculated from magnetic field data and particle data might be because ESAs do not cover the full energy range of high-energy ion precipitation.

[20] We estimated the intensity of FAC at 2220:51–2220:54 UT, when the electron fluxes were significantly enhanced (Figure 5a), from the magnetic field variation in Figure 5g as  $J = (\nabla \times \mathbf{B}) / \mu_0$ , where  $J$ ,  $\mu_0$ , and  $\mathbf{B}$  are the current, permeability of vacuum, and magnetic field, respectively. The intensity of the FAC ( $\sim 16 \mu\text{A}/\text{m}^2$ ) is extremely large compared with the typical FACs in the auroral zone ( $\sim 1 \mu\text{A}/\text{m}^2$ ).

#### 3.3. Electron Energy Distribution

[21] To illustrate the spectral features of BBEs in detail, Figure 6 shows the energy spectra of downward electrons (pitch angles within  $\pm 15^{\circ}$ ) at four times: (1) 2220:12 UT, (2) 2220:42 UT, (3) 2221:35 UT, and (4) 2223:46 UT. These times are indicated by arrows in Figure 5a. Times 1 and 2 are in the BBEs. Crosses on the energy spectrum time 1 indicate the energy steps of ESAs, which are the same for all four

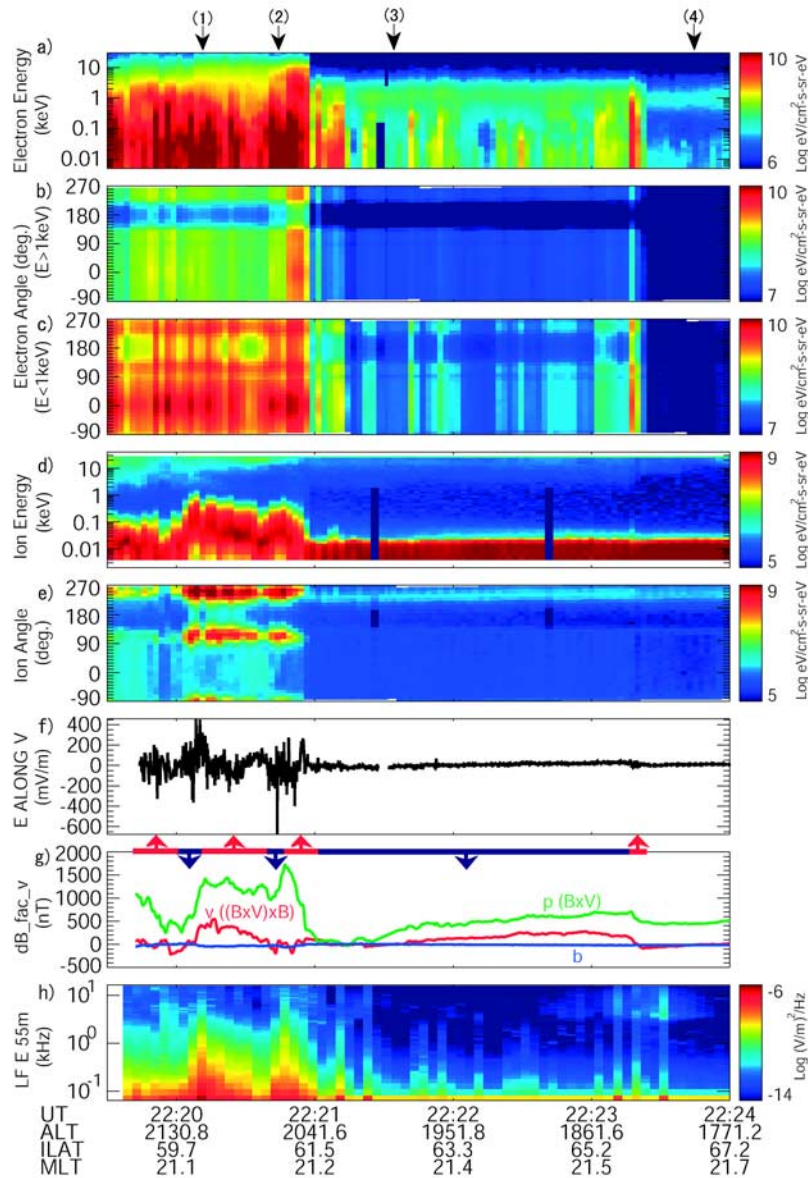


**Figure 5.** From top to bottom, (a) energy–time spectrograms of downward electrons (pitch angles within  $\pm 15^\circ$ ), pitch angle distributions of electrons at energy range (b) above 1 keV and (c) below 1 keV, (d) energy–time spectrograms and (e) pitch angle distributions of ions, (f) electric field measured along the spacecraft orbit (nearly north–south), (g) magnetic field fluctuations (blue line: field-aligned component, green line: nearly east–west, and red line: nearly north–south), and (h) wave spectra (electric field) observed by the FAST satellite at 2219:30–2224:00 UT on 15 July 2000. The black arrows above Figure 5a indicate the times when the electron energy spectra in Figure 6 and pitch angle distributions in Figure 7 are obtained. The arrows and lines in Figure 5g indicate directions of FACs (red is upward and blue is downward), which are estimated by the latitudinal gradient of magnetic field variations in the component of  $p(\mathbf{B} \times \mathbf{V})$ .

spectra. Energy fluxes of BBEs [times 1 and 2] were larger than those at higher latitudes [times 3 and 4] at the measured energy ranges. The energy spectrum time 2 at 2220:42 UT had a small peak at  $\sim 4$  keV. Such a peak is not prominent in spectrum time 1 at 2220:12 UT. Similar small peaks are found around this time at 2220:42–2220:52 UT, when intense fluxes are particularly observed at all measured energy ranges, as shown in Figure 5a. We tried to fit the Maxwellian distribution function to the observed energy spectra for the energy ranges above and below the peaks separately. How-

ever, the spectra of the BBEs did not fit to the Maxwellian distribution for either the energy ranges. Energy spectra of times 3 and 4 showed features of plasma sheet electrons with a peak at  $\sim 1$  keV. These features of plasma sheet electrons are continuously identified in the energy–time spectrograms at 2220:55–2225:10 UT (Figure 1b).

### 3.4. Pitch Angle Distribution

[22] Figure 7 shows the pitch angle distributions of electrons observed by the FAST satellite at the four times

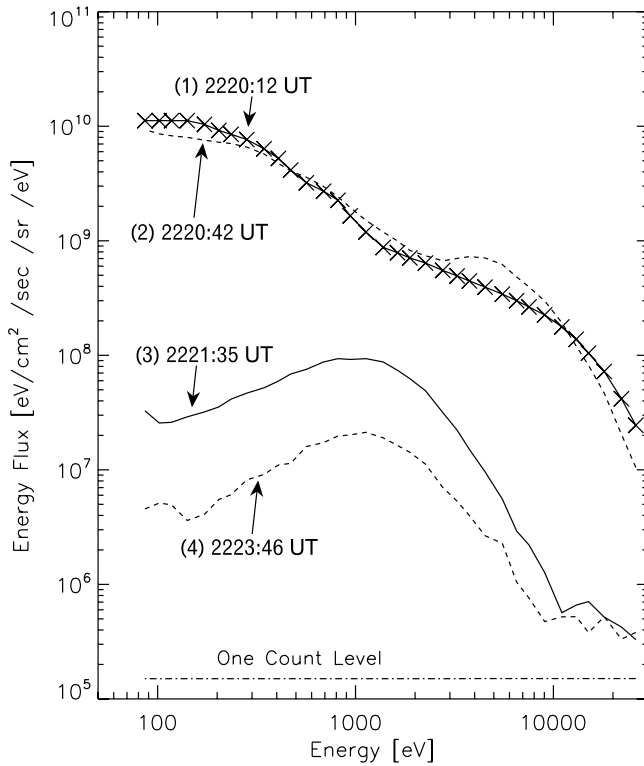


**Figure 6.** Downward electron energy spectra parallel to the local magnetic field (pitch angles within  $\pm 15^\circ$ ) observed by the FAST satellite at (1) 2220:12 UT, (2) 2220:42 UT, (3) 2221:35 UT, and (4) 2223:46 UT on 15 July 2000. These times are indicated by arrows in Figure 5a.

shown by the arrows in Figure 5a. The pitch angle in the horizontal axis is determined for the local magnetic field, where  $0^\circ$  is downward parallel flux,  $\pm 180^\circ$  are upward parallel flux, and  $\pm 90^\circ$  are flux perpendicular to the local magnetic field. Small squares on pitch angle distributions of 0.05 keV are the data points of ESAs, which are the same for pitch angle distributions at all energy levels.

[23] Energy fluxes of BBEs [times 1 and 2] are larger than those at higher latitudes [times 3 and 4] at all measured pitch angles of the each energy. At a lower energy range below 0.47 keV in times 1 and 2 during the BBE event, parallel electron fluxes are larger than perpendicular fluxes and electron fluxes at the pitch angles of  $\sim 120^\circ$  and  $\sim 240^\circ$  tend to be also enhanced. Enhanced field-aligned upward electron fluxes are observed associated with more intense downward fluxes at an energy of 0.05 keV at time 2 2220:42 UT and those are sometimes seen during the BBE event (Figure 5c). In contrast, at a higher energy range above 1.10 keV, electron fluxes show isotropic features between  $-130^\circ$  and  $130^\circ$  and loss cone features at  $>130^\circ$  and  $<-130^\circ$ . These features are mostly identified during the BBE event at 2219:30–2220:55 UT (Figures 5b and 5c). These different characteristics of pitch angle distribution at lower and higher energy ranges suggest that the BBEs consist of two energy components. For the plasma sheet electrons shown in times 3 and 4, pitch angle distributions below 0.10 keV were mostly isotropic over all pitch angles. At energy ranges above 0.47 keV, the pitch angle distributions were mostly isotropic at pitch

angles within  $\pm 130^\circ$ , although the fluxes came close to the one-count level. Energy spectra at higher latitudes at 2220:55–2223:20 UT and 2223:20–2225:10 UT had pitch angle distributions mostly similar to those shown in times 3 and 4, respectively.

### 3.5. Moment Calculation

[24] In Figures 8b and 8c, we show the time variations of thermal energies and densities of electrons obtained by moment calculations of the observed electron distributions. The energy–time spectrograms, including the BBEs at 2219:30–2220:55 UT, are reproduced in Figure 8a. The solid and dashed lines indicate the parameters obtained for the energy ranges above and below 1 keV during the BBE event, respectively. The solid lines at 2220:55–2221:30 UT represent estimated parameters for plasma sheet electrons at higher latitudes for all the energy ranges of 0.08–30 keV. During the BBEs at 2219:30–2220:55 UT, the thermal energy (1.2–2.0 keV) at the higher energy range were larger than those estimated for the plasma sheet electrons at higher latitudes (below 1 keV). The densities at lower and higher energy ranges for the BBEs are estimated to be  $30\text{--}150\text{ cm}^{-3}$  and  $3\text{--}30\text{ cm}^{-3}$ , respectively. The large densities at the lower energy part of BBEs suggest that the source plasma of BBEs is not only the plasma sheet electrons.

### 3.6. Waves

[25] As shown in Figure 5e, intense fluctuations of the electric field with an amplitude of more than 100 mV/m are observed during the BBE event. These low-frequency waves may contribute to the acceleration of BBEs through wave–particle interactions. In that case, the wave energy flux (Poynting flux) may correlate with electron energy flux. To check this situation, we compare the time variation of Poynting flux (solid curve) and field-aligned electron energy flux (dashed curve) in Figure 8d. Positive fluxes are downward. The Poynting fluxes are calculated by the cross-product  $\mathbf{E} \times \mathbf{B} / \mu_0$ . We used the electric field ( $\mathbf{E}$ ), which is averaged to 8 Hz from the original 32-Hz data in the component along the satellite track (nearly north–south, northward positive) and 8 Hz sampled magnetic field ( $\mathbf{B}$ ) data in the component of  $p(\mathbf{B} \times \mathbf{V})$  (nearly east–west, eastward positive). The FAST satellite does not measure the other component (east–west) of the electric field. The magnetic field data may contain the effect of spatial variations of FACs rather than temporal variations by waves. To remove the effects of lower frequency variations including FACs, we subtracted a running average of 16 s from these electric and magnetic field data, respectively. These “detrended” electric and magnetic field data are plotted in Figures 8e and 8f, respectively. The time variation of Poynting flux calculated by these detrended fields is shown by the solid curve in Figure 8d. Here we compare the Poynting flux with the total electron energy fluxes (dashed curve), which are calculated from the electron fluxes over a lower energy range below 1 keV. From the pitch angle distribution in Figures 5b, 5c, and 7, we consider that the lower energy part of BBEs may be accelerated by low-frequency waves near the satellite altitudes.

[26] In Figure 8d, the Poynting flux shows higher frequency variations compared with electron flux variations. This is due to the different sampling rate of the data

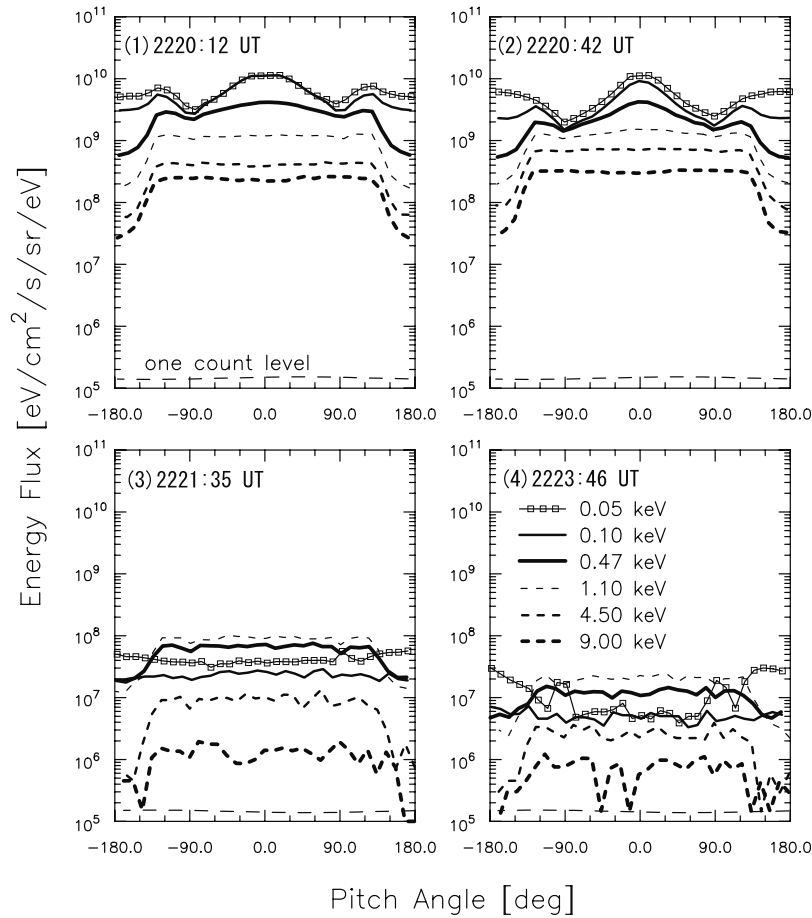


**Figure 7.** Pitch angle distributions of electron energy fluxes at (1) 2220:12 UT, (2) 2220:42 UT, (3) 2221:35 UT, and (4) 2223:46 UT. These times are indicated by arrows in Figure 5a. The horizontal axis indicates the pitch angle to the local magnetic field, where the center (0.0) and edges ( $\pm 180.0$ ) correspond to the field-aligned downward and upward fluxes, respectively.

(Poynting flux: 0.13 s, electron flux: 2.5 s). When the electron energy flux is enhanced, the amplitudes of fluctuating Poynting flux tend to become large. However, while the Poynting fluxes have both upward and downward directions, the electron fluxes are downward. There is no clear correlation between electron energy flux and Poynting flux during the BBE event. We also calculated downward and upward electron energy fluxes separately. The variations of downward and upward fluxes also do not have obvious correlation with those of the Poynting flux.

[27] Figure 9 shows the wave power spectra at frequencies of 0.06–4.0 Hz obtained by the Fast Fourier Transform (FFT) of the electric field in Figure 5f, the magnetic field in Figure 5g ( $p(\mathbf{B} \times \mathbf{V})$  component), and the Poynting flux. Solid and dashed curves are power spectra during the BBE event (2219:47–2220:51 UT) and those in the higher latitude plasma sheet electrons (2220:58–2222:27 UT), respectively. At all frequencies, the wave powers of the electric field, the magnetic field, and the Poynting flux during the BBE event are more intense than those at higher latitudes. Significant peak is not seen in these spectra.

[28] Figure 10 shows wave spectra at higher frequencies of 0.016–16 kHz shown in Figure 5h at 2219:38–2220:54 UT during the BBE event (solid curve) and at 2220:58–

2222:15 UT at higher latitudes (dotted curve). These spectra are averages of 20 spectra observed every  $\sim 4$  s. At all measured frequency ranges, wave powers were clearly enhanced during the BBE event without a particular peak. The slope of the spectrum during the BBE event is  $\sim f^{-2}$  and is softer compared with the slope of the spectrum at higher latitudes ( $\sim f^{-4}$  below 0.2 kHz and  $\sim f^{-3}$  above 0.2 kHz).

[29] The signature of enhanced wave power in this frequency range is often referred to as broadband extremely low-frequency (BBELF) turbulence [Norqvist *et al.*, 1998]. Bouhram *et al.* [2002] reported that using Freja and FAST data ion-heating event in the midaltitude auroral zone were correlated with enhanced emissions in the BBELF range. The intense perpendicular ion fluxes below  $\sim 1$  keV were observed during our event (Figure 5d). Enhanced BBELF waves shown in Figures 5h and 10 are associated with perpendicular ion fluxes shown in Figure 5e.

## 4. Discussion

### 4.1. Duration and Width

[30] BBEs were observed at 2219:30–2220:55 UT,  $59^\circ$ – $61^\circ$  ILAT, and 21 MLT on 15 July 2000 (Figure 1b). The BBEs were not observed in one orbit before and after the

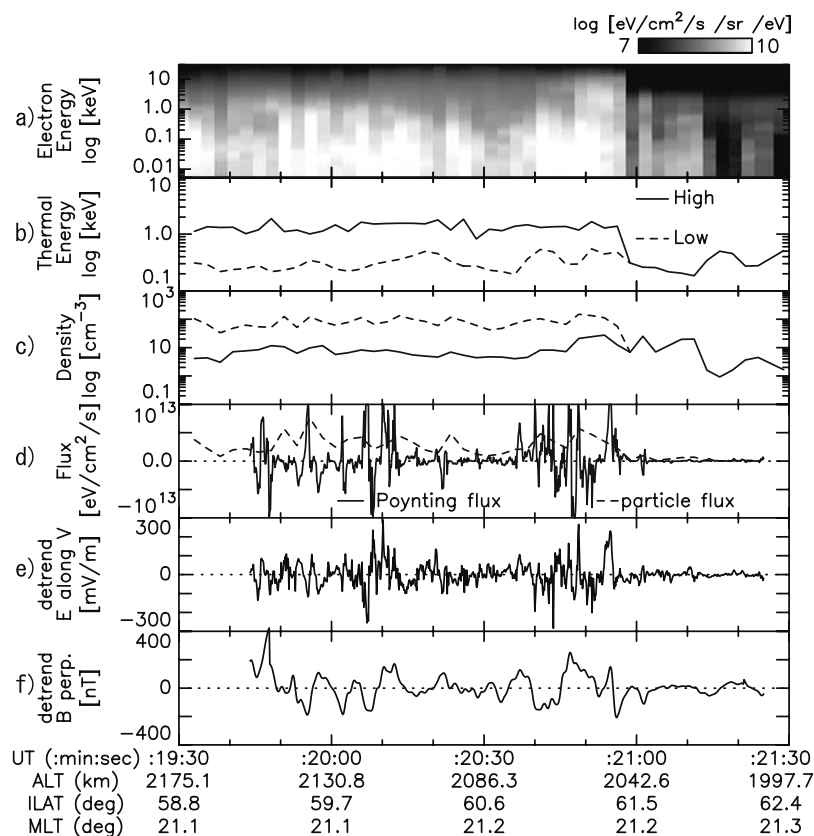


**Figure 8.** From top to bottom, (a) energy–time spectrograms of downward electrons, parameters obtained by moment calculation from electron data [(b) thermal energy and (c) density], (d) Poynting flux (solid curve,  $\mathbf{E} \times \mathbf{B} / \mu_0$  using detrended  $\mathbf{E}$  in Figure 8e and detrended  $\mathbf{B}$  in Figure 8f, respectively) and total energy fluxes (dashed curve) estimated from electron fluxes at a lower energy range below 1 keV, and (e) detrended  $\mathbf{E}$  and (f) detrended  $\mathbf{B}$  obtained by subtracting running averages of 16 s from electric field measured along the spacecraft orbit in Figure 5f (nearly north–south) and magnetic field in the component of  $p(\mathbf{B} \times \mathbf{V})$  in Figure 5g (nearly east–west), respectively.

pass in the same MLAT and MLT region (Figure 1). From the timescale of the FAST orbital period ( $\sim 133$  min), the duration of the BBEs is less than  $\sim 4$  hours.

[31] In this paper, we first compared the precipitating region of the BBEs with the global auroral images obtained by the Polar UVI imager in Figure 4, giving further evidence of the duration and spatial extent of the BBEs. A local intensification of UVI auroral emission occurred at 2218:21 UT at  $50^\circ$ – $60^\circ$  MLAT and 20–21 MLT,  $\sim 5$  min after the substorm onset. The FAST satellite crossed this local emission region and observed the BBEs at 2219:30–2220:55 UT. The intensification of the aurora lasted  $\sim 14$  min, until 2232:27 UT, in this region. We conclude that the duration of this BBE event was  $\sim 14$  min. Comparison with the global auroral images also indicates that the precipitating region of BBEs was at  $50^\circ$ – $60^\circ$  MLAT and 20–21 MLT, with longitudinal widths of  $\sim 15^\circ$ . Based upon multisatellite measurements of BBEs, *Shiokawa et al.* [1997] concluded that BBEs were observed at  $47^\circ$ – $66^\circ$  MLAT with latitudinal widths of  $2^\circ$ – $9^\circ$  and usually lasted for less than 30 min. These temporal and latitudinal widths agree with our results using the Polar UVI images.

## 4.2. Acceleration Region

[32] In this paper, we showed the pitch angle distribution of BBEs using FAST data for the first time. At a higher energy range above  $\sim 1$  keV, the energy spectra of BBEs showed isotropic distributions in the local magnetic field with a loss cone feature, as shown in Figures 5b and 7. This result shows that the higher energy parts of the BBEs are accelerated at higher altitudes in the inner magnetosphere, because the pitch angle distribution of higher energy electrons originating in the magnetosphere tends to become isotropic due to the mirror force as they approach the ionosphere. On the dipole magnetic field model of the earth, only electrons with pitch angles less than  $5.1^\circ$  at the equatorial plane of the inner magnetosphere can reach an altitude of  $\sim 2000$  km at  $60^\circ$  ILAT along the magnetic field line.

[33] At a lower energy range below  $\sim 1$  keV, the field-aligned electron fluxes of BBEs were more intense than the perpendicular fluxes (Figures 5c and 7). This result suggests that the lower energy part of BBEs is accelerated parallel to the local magnetic field at low altitudes near the satellite ( $\sim 2000$  km). From these different characteristics of pitch angle distribution and from the spectral shapes of the BBEs with small peaks at  $\sim 4$  keV at 2220:42–2220:52 UT, we

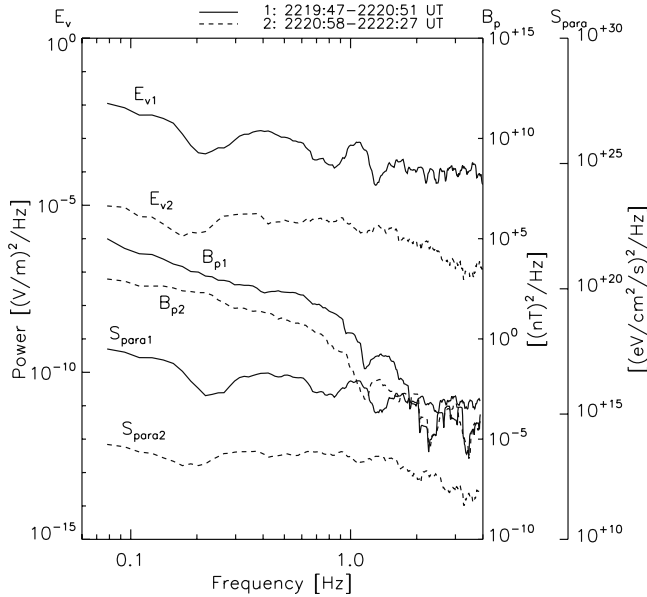


**Figure 9.** Wave spectra of the electric field ( $E_v$ ) in Figure 5f, the magnetic field ( $B_p$ ) in Figure 5g ( $p(\mathbf{B} \times \mathbf{V})$  component), and the Poynting flux ( $S_{para}$ ) in Figure 8d at frequencies of 0.06–4.0 Hz obtained by the FAST satellite on 15 July 2000. The solid and dashed curves indicate wave spectra at 2219:47–2220:51 UT during the BBE event and at 2220:58–2222:27 UT at higher latitudes, respectively.

conclude that the BBEs consist of two energy components, which are accelerated at two different altitudes.

### 4.3. Acceleration Mechanism

[34] The monoenergetic peak of precipitating electron spectra is often observed in the discrete auroral region, indicating the acceleration of electrons by the upward field-aligned potential difference [Frank and Ackerson, 1971]. The energy spectra of BBEs without monoenergetic peaks show that both the higher and lower energy parts of BBEs are accelerated by some kind of waves or field fluctuations rather than by field-aligned potential differences.

[35] Theoretical studies suggest that kinetic Alfvén waves could provide a mechanism to transfer wave energy to particle energy [Hasegawa, 1976; Goertz, 1984]. Keiling *et al.* [2002] showed that the energy flux of Alfvén waves is sufficient to account for magnetically conjugate low-altitude auroral phenomena using data from the Polar satellite.

[36] Precipitating electrons with a wide energy range, similar to the BBEs studied in this paper, are often observed near the poleward boundary of the auroral oval [e.g., Nagatsuma *et al.*, 1995, 1996; Dombeck *et al.*, 2005]. Dombeck *et al.* [2005] reported simultaneous observations of Alfvén waves and auroral electrons at Polar and FAST altitudes,  $\sim 7 R_e$  geocentric and  $\sim 3500$  km, respectively, at  $\sim 23$  MLT in the main phase of a storm on 22 October 1999. They showed that electrons over a wide energy range were observed at FAST altitudes on field lines that map to the plasma sheet boundary layer. They also showed evidence for acceleration of electrons by Alfvén waves between Polar and FAST. Nagatsuma *et al.* [1995] concluded using data from the Akebono satellite that the energy spectra with a wide energy range at the poleward boundary of oval are charac-

terized by a superposition of two Maxwellian functions: isotropic high-temperature component and field-aligned low-temperature component (suprathermal electrons). These pitch angle features are similar to those of the BBEs studied here. However, as shown in Figure 6, the energy spectra of both higher and lower energy components of the BBEs do not fit to the Maxwellian distribution.

[37] The isotropic pitch angle distribution for the higher energy part of BBEs, the relation to the substorm onset, and the clear poleward boundary of the BBEs at  $\sim 61^\circ$  suggest that the higher energy part of the BBEs are accelerated by some unknown mechanism in the inner magnetosphere associated with the storm-time substorm.

[38] Next, we discuss the lower energy part of the BBEs. The suprathermal electron bursts have somewhat similar characteristics to those of the BBEs at the lower energy range. Johnstone and Winningham [1982] reported a detailed study of suprathermal electron bursts observed by the ISIS-2 satellite. The suprathermal electron bursts are intense flux enhancements of precipitating electrons at a lower energy range below a few kiloelectron volts. The electron flux has a peak in a field-aligned direction during the suprathermal electron bursts. These features are similar to those of the lower energy part of the BBEs studied in this paper. However, the latitudinal width of suprathermal electron burst (typically

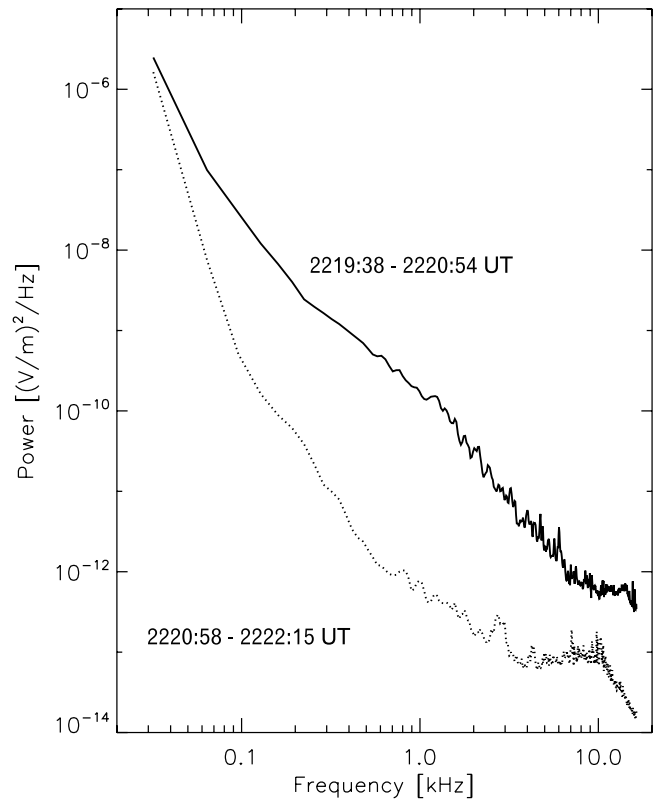


**Figure 10.** Wave spectra in the electric field at frequencies of 0.016–16 kHz observed by the FAST satellite. The solid and dotted curves indicate the spectrum at 2219:38–2220:54 UT during the BBE event and at 2220:58–2222:15 UT at higher latitudes. The satellite measured the wave spectrum every  $\sim 4$  s. Twenty spectra are averaged in these curves.

$\sim 20$  km) is much smaller than that of the BBEs, which were observed at least  $\sim 2.0^\circ$  in latitude ( $\sim 200$  km) by the FAST satellite.

[39] *Watt et al.* [2005, 2006] simulated field-aligned downward electron acceleration through interaction between electrons and inertial shear Alfvén waves at altitudes between 800 km and  $2.5 R_E$ . They compared the simulation results with FAST observations at an altitude of  $\sim 3200$  km. During their event, the time variations of electron pitch angle distribution observed by FAST show specific signatures of field-aligned fluxes, which are similar to the simulation results. The pitch angle distributions at a lower energy range during the BBE event are similar to the observations in Figure 2e of *Watt et al.* [2006].

[40] *Mende et al.* [2003] showed the spectral characteristics of precipitating electrons observed 1 min after a nonstorm time substorm onset using the FAST satellite data. They showed the aurora associated with the substorm initial brightening is dominated by intense field-aligned electron fluxes at suprathermal energies, showing typical properties of electrons accelerated by Alfvén waves. The electron features they reported are similar to those of the lower energy part of the BBEs, which are observed shortly after a storm-time substorm.

[41] The pitch angle distributions at a lower energy range have a peak in the field-aligned direction during our BBE event. Intense fluctuations of the electric and magnetic fields at 0.06–4.0 Hz are observed by the FAST satellite during this event, as shown in Figures 5f, 5g, and 9. Enhanced waves (electric field) are also observed at frequency range of 0.016–16.0 kHz (Figures 10). These results suggest that the lower energy part of BBEs is accelerated along the magnetic field line through the wave–particle interaction at altitudes near the FAST satellite. However, clear correlation is not found between electron energy flux of lower energy part of BBEs and wave Poynting flux at 0.06–4.0 Hz (Figure 8d). This fact may be because the acceleration by waves occurs not at the satellite altitude but at altitudes higher than the satellite or because the acceleration occurs at different frequency range.

[42] In Figures 5c and 7, enhanced field-aligned upward electron fluxes are sometimes observed associated with more intense downward fluxes at the lower energy range below 1 keV during the BBE event. These upward fluxes possibly consist of ionospheric secondary electrons, which are isotropically generated by collisions between precipitating electrons and atmosphere and move upward due to the mirror force. The upward electrons may be accelerated in the field-aligned direction. The observed Poynting fluxes have components not only downward but also upward during the BBE event. The upward component of Poynting flux might contribute to the enhanced upward fluxes. However, upward electron energy flux does not show clear correlation with the Poynting flux, as noted above.

## 5. Summary and Conclusion

[43] We have studied a broadband electron (BBE) event observed on 15 July 2000, during a large geomagnetic storm, using data from the FAST satellite, the ground magnetometers, and the Polar UVI. The characteristics of the BBEs are summarized as follows.

[44] 1. The BBEs were observed at  $59^\circ$ – $61^\circ$  ILAT and 21 MLT during the main phase of a large geomagnetic storm with a minimum *Dst* index of  $-301$  nT. Electron energy fluxes during this BBE event were larger than those at higher latitudes at all measured energy ranges. Ground magnetometer data around 21 MLT show that a substorm started from  $\sim 7$  min before the BBE event. BBEs were not observed one pass ( $\sim 133$  min) before and after the event in the same ILAT and MLT region. In addition, a localized intensification of auroral emission is identified in the Polar UVI images at  $50^\circ$ – $60^\circ$  MLAT and 20–21 MLT at the ionospheric footprint of the BBEs. The duration of the intensification was  $\sim 14$  min. Based on these results, we conclude that the acceleration of the BBEs occurred in association with a substorm during the main phase of the storm at  $50^\circ$ – $60^\circ$  MLAT and 20–21 MLT, lasting for  $\sim 14$  min.

[45] 2. The variation of the magnetic field indicated that the precipitation region of BBEs corresponded to the intense FACs with complicated structures of both upward and downward directions at equatorward of the steady downward current region in the premidnight sector.

[46] 3. Electron fluxes at a higher energy range above  $\sim 1$  keV show isotropic and loss cone features during the BBE event. At a lower energy range below  $\sim 1$  keV, field-aligned electron fluxes tended to be higher than perpendicular fluxes. We conclude that the higher energy part of the BBEs is accelerated in the inner magnetosphere, and the lower energy part is accelerated parallel to the local magnetic field at lower altitudes near the satellite ( $\sim 2000$  km). These results also imply that the BBEs consist of two energy components.

[47] 4. The energy spectra of the BBEs do not have monoenergetic peaks. The amplitudes of electric and magnetic fluctuations are very large ( $\sim 200$  mV/m and  $\sim 500$  nT, respectively) during the BBE event. The wave spectra show intensified wave power at all frequency ranges of 0.06–4.0 Hz and 0.016–16 kHz. From these results, we suggest acceleration of the lower energy part of the BBEs through wave–particle interaction near the satellite. However, wave Poynting flux at 0.06–4.0 Hz takes both upward and downward directions and does not have clear correlation with electron energy flux of lower energy range of the BBEs.

[48] 5. The ion fluxes below  $\sim 1$  keV and above  $\sim 10$  keV were enhanced during the BBE event. The intense ion fluxes below  $\sim 1$  keV are mainly in perpendicular direction to the local magnetic field. The enhanced BBELF waves at 0.016–16 kHz may contribute to create the observed intense perpendicular ion fluxes.

[49] **Acknowledgments.** This work is supported by a grant from the Ministry of Education, Culture, Sports, Science and Technology, Japan (Dynamics of the Sun-Earth-Life Interactive System, No. G-4, the 21st Century COE Program). The *Dst* index and geomagnetic H-component data obtained by the ground-based stations were provided by the World Data Center-C2 for Geomagnetism, Kyoto University. High time-resolution (1 s) magnetic field data obtained at Hermanus (HER) were provided by Peter Sutcliffe of the Hermanus Magnetic Observatory. The Polar UVI data were provided by George Parks of the University of Washington.

[50] Zuyin Pu thanks Patrick T. Newell and Claire Watt for their assistance in evaluating this paper.

## References

Bouhram, M., et al. (2002), Ion outflow and associated perpendicular heating in the cusp observed by interball auroral probe and Fast Auroral Snapshot, *J. Geophys. Res.*, *107*(A2), 1023, doi:10.1029/2001JA000091.

- Carlson, C. W., R. F. Pfaff, and J. G. Watzin (1998), The Fast Auroral Snapshot (FAST) mission, *Geophys. Res. Lett.*, *25*(12), 2013–2016.
- Carlson, C. W., J. P. McFadden, P. Turin, D. W. Curtis, and A. Magoncelli (2001), The electrons and ion plasma experiment for FAST, *Space Sci. Rev.*, *98*, 33–66.
- Chen, M. W., M. Schulz, P. C. Anderson, G. Lu, G. Germany, and M. Wüest (2005), Storm time distributions of diffuse auroral electron energy and X-ray flux: Comparison of drift-loss simulations with observations, *J. Geophys. Res.*, *110*(A3), A03210, doi:10.1029/2004JA010725.
- Cheng, C.-C., C. T. Russell, Y. F. Gao, and P. J. Chi (2002), On consecutive bursts of low-latitude Pi 2 pulsations, *J. Atmos. Sol. Terr. Phys.*, *64*, 1809–1821.
- Cheng, C.-C., C. T. Russell, K. Yumoto, Y. F. Gao, and P. J. Chi (2004), Characteristics of consecutive bursts of Pi 2 pulsations observed at the SMALL array: A new implication, *Earth Planets Space*, *56*, 531–545.
- Denig, W. F., and F. J. Rich (1986), The ionosphere–magnetosphere structure during a geomagnetic storm based on measurements in the morning auroral zone, *J. Geophys. Res.*, *91*(A1), 165–182.
- Dombeck, J., C. Cattell, J. R. Wygant, A. Keiling, and J. Scudder (2005), Alfvén waves and Poynting flux observed simultaneously by Polar and FAST in the plasma sheet boundary layer, *J. Geophys. Res.*, *110*(A12S90), doi:10.1029/2005JA011269.
- Egeland, A., W. J. Burke, N. C. Maynard, E. M. Basinska, J. D. Winningham, and C. S. Deehr (1994), Ground and satellite observations of postdawn aurorae near the time of a sudden storm commencement, *J. Geophys. Res.*, *99*(A2), 2095–2108.
- Elphic, R. C., J. D. Means, R. C. Snare, R. J. Strangeway, L. Kepko, and R. E. Ergun (2001), Magnetic field instruments for the Fast Auroral Snapshot explorer, *Space Sci. Rev.*, *98*, 151–168.
- Ergun, R. E., et al. (2001), The FAST satellite fields instrument, *Space Sci. Rev.*, *98*, 67–91.
- Frank, L. A., and K. L. Ackerson (1971), Observations of charged particle precipitation into the auroral zone, *J. Geophys. Res.*, *76*(16), 3612–3643.
- Goertz, C. K. (1984), Kinetic Alfvén waves on auroral field lines, *Planet. Space Sci.*, *32*(11), 1387–1392.
- Gussenhoven, M. S., D. A. Hardy, and W. J. Burke (1981), DMSP/F2 electron observations of equatorward auroral boundaries and their relationship to magnetospheric electric fields, *J. Geophys. Res.*, *86*(A2), 768–778.
- Hardy, D. A., M. S. Gussenhoven, and E. Holeman (1985), A statistical model of auroral electron precipitation, *J. Geophys. Res.*, *90*(A5), 4229–4248.
- Hasegawa, A. (1976), Particle acceleration by MHD surface wave and formation of aurora, *J. Geophys. Res.*, *81*(28), 5083–5090.
- Johnstone, A. D., and J. D. Winningham (1982), Satellite observations of suprathermal electron bursts, *J. Geophys. Res.*, *87*(A4), 2321–2329.
- Keiling, A., J. R. Wygant, C. Cattell, W. Peria, G. Parks, M. Temerin, F. S. Mozer, C. T. Russell, and C. A. Kletzing (2002), Correlation of Alfvén wave Poynting flux in the plasma sheet at 4–7  $R_E$  with ionospheric electron energy flux, *J. Geophys. Res.*, *107*(A7), 1132, doi:10.1029/2001JA900140.
- Mende, S. B., C. W. Carlson, H. U. Fray, L. M. Peticolas, and N. Østgaard (2003), FAST and IMAGE-FUV observations of a substorm onset, *J. Geophys. Res.*, *108*(A9), 1344, doi:10.1029/2002JA009787.
- Nagatsuma, T., H. Fukunishi, and T. Mukai (1995), Spatial relationships between field-aligned currents and suprathermal electron beams observed at the poleward boundary of the nightside auroral oval, *J. Geophys. Res.*, *100*(A2), 1625–1637.
- Nagatsuma, T., H. Fukunishi, H. Hayakawa, T. Mukai, and A. Matsuoka (1996), Field-aligned currents associated with Alfvén waves in the poleward boundary region of the nightside auroral oval, *J. Geophys. Res.*, *101*(A10), 21,715–21,729.
- Nishino, M., K. Makita, K. Yumoto, Y. Miyoshi, N. J. Schuch, and M. A. Abdu (2006), Energetic particle precipitation in the Brazilian geomagnetic anomaly during the “Bastille Day storm” of July 2000, *Earth Planets Space*, *58*, 607–616.
- Norqvist, P., M. André, and M. Tyrlund (1998), A statistical study of ion energization mechanisms in the auroral region, *J. Geophys. Res.*, *103*(A10), 23,459–23,473.
- Rastätter, L., M. Hesse, M. Kuznetsova, T. I. Gombosi, and D. L. DeZeeuw (2002), Magnetic field topology during July 14–16 2000 (Bastille Day) solar CME event, *Geophys. Res. Lett.*, *29*(15), 1747, doi:10.1029/2001GL014136.
- Sharber, J. R., et al. (1998), UARS particle environment monitor observations during the November 1993 storm: Auroral morphology, spectral characterization, and energy deposition, *J. Geophys. Res.*, *103*(A11), 26,307–26,322.
- Shiokawa, K., K. Yumoto, C.-I. Meng, and G. Reeves (1996), Broadband electrons observed by the DMSP satellites during storm-time substorms, *Geophys. Res. Lett.*, *23*(18), 2529–2532.
- Shiokawa, K., C.-I. Meng, G. D. Reeves, F. J. Rich, and K. Yumoto (1997), A multievent study of broadband electrons observed by the DMSP satellites and their relation to red aurora observed at midlatitude stations, *J. Geophys. Res.*, *102*(A7), 14,237–14,253.
- Shiokawa, K., R. R. Anderson, I. A. Daglis, W. J. Hughes, and J. R. Wygant (1999), Simultaneous DMSP and CRRES observation of broadband electrons during a storm-time substorm on March 25, 1991, *Phys. Chem. Earth*, *24*, 281–285.
- Spiro, R. W., P. H. Reiff, and L. J. Maher Jr. (1982), Precipitating electron energy flux and auroral zone conductances: An empirical model, *J. Geophys. Res.*, *87*(A10), 8215–8227.
- Torr, M. R., et al. (1995), A far ultraviolet imager for the international solar-terrestrial physics mission, *Space Sci. Rev.*, *71*, 329–383.
- Watt, C. E. J., R. Rankin, I. J. Rae, and D. M. Wright (2005), Self-consistent electron acceleration due to inertial Alfvén wave pulses, *J. Geophys. Res.*, *110*, A10S07, doi:10.1029/2004JA010877.
- Watt, C. E. J., R. Rankin, I. J. Rae, and D. M. Wright (2006), Inertial Alfvén waves and acceleration of electrons in nonuniform magnetic fields, *Geophys. Res. Lett.*, *33*, L02106, doi:10.1029/2005GL024779.
- Yumoto, K., K. Takahashi, T. Saito, F. W. Menk, B. J. Fraser, T. A. Potemra, and L. J. Zanetti (1989), Some aspects of the relation between Pi 1-2 magnetic pulsations observed at  $L = 1.3–2.1$  in the ground and substorm-associated magnetic field variations in the near-earth magnetotail observed by AMPTE/CCE, *J. Geophys. Res.*, *94*(A4), 3611–3618.
- Yumoto, K., and the CPMN Group (2001), Characteristics of Pi 2 magnetic pulsations observed at the CPMN stations: A review of the STEP results, *Earth Planets Space*, *53*, 981–992.

C. W. Carlson and J. P. McFadden, Space Sciences Laboratory, University of California Berkeley, Berkeley, CA 94720–7450, USA. (cwc@apollo.ssl.berkeley.edu; mcfadden@apollo.ssl.berkeley.edu)

A. Nakajima, K. Seki, and K. Shiokawa, Solar-Terrestrial Environment Laboratory, Nagoya University, Honohara, Toyokawa 442–8507, Japan. (akimitsu@stelab.nagoya-u.ac.jp; seki@stelab.nagoya-u.ac.jp; shiokawa@stelab.nagoya-u.ac.jp)

R. J. Strangeway, Institute of Geophysics and Planetary Physics, University of California Los Angeles, Los Angeles, CA 90024–1567, USA. (strange@igpp.ucla.edu)